



Contents lists available at ScienceDirect

Surface Science

journal homepage: [www.elsevier.com/locate/susc](http://www.elsevier.com/locate/susc)

## Initial stages of the autocatalytic oxidation of the $\text{InAs}(001)-(4 \times 2)/c(8 \times 2)$ surface by molecular oxygen

Jonathon B. Clemens<sup>a</sup>, Sarah R. Bishop<sup>a</sup>, Darby L. Feldwinn<sup>a,1</sup>, Ravi Droopad<sup>b,2</sup>, Andrew C. Kummel<sup>a,\*</sup>

<sup>a</sup> Department of Chemistry and Biochemistry, University of California, San Diego, 9500 Gilman Dr., #0358, La Jolla, CA 92093-0358, USA

<sup>b</sup> Freescale Semiconductor, 2100 E. Elliot Road, Tempe, AZ 85283, USA

### ARTICLE INFO

#### Article history:

Received 3 March 2009

Accepted for publication 27 April 2009

Available online xxx

#### Keywords:

Density functional calculations

Monte Carlo simulations

Scanning tunneling microscopy

Chemisorption

Oxidation

Indium arsenide

Oxygen

Semi conducting surfaces

### ABSTRACT

The initial stages of oxidation of the In-rich  $\text{InAs}(001)-(4 \times 2)/c(8 \times 2)$  surface by molecular oxygen ( $\text{O}_2$ ) were studied using scanning tunneling microscopy (STM) and density functional theory (DFT). It was shown that the  $\text{O}_2$  dissociatively chemisorbs along the rows in the  $[110]$  direction on the InAs surface either by displacing the row-edge As atoms or by inserting between In atoms on the rows. The dissociative chemisorption is consistent with being autocatalytic: there is a high tendency to form oxygen chemisorption sites which grow in length along the rows in the  $[110]$  direction at preexisting oxygen chemisorption sites. The most common site size is about 21–24 Å in length at ~25% ML coverage, representing 2–3 unit cell lengths in the  $[110]$  direction (the length of ~5–6 In atoms on the row). The autocatalysis was confirmed by modeling the site distribution as non-Poisson. The autocatalysis and the low sticking probability ( $\sim 10^{-4}$ ) of  $\text{O}_2$  on the  $\text{InAs}(001)-(4 \times 2)/c(8 \times 2)$  are consistent with activated dissociative chemisorption. The results show that it is critical to protect the InAs surface from oxygen during subsequent atomic layer deposition (ALD) or molecular beam epitaxy (MBE) oxide growth since oxygen will displace As atoms.

© 2009 Elsevier B.V. All rights reserved.

### 1. Introduction

As complementary metal-oxide-semiconductor (CMOS) technology approaches the 22 nm node, new channel materials may be included in metal-oxide-semiconductor field effect transistors (MOSFETs) in order to improve device performance while decreasing the average feature sizes. InAs is being investigated for III–V MOSFETs using high- $\kappa$  dielectrics ( $\text{Al}_2\text{O}_3$ ) [1]. InAs is also used as a channel layer in III–V HEMTs due to its high electron mobility and the ease of growing InAs on wider band gap substrates such as InP using lateral overgrowth molecular beam epitaxy [2].

In ALD, most gate oxides are deposited using water, peroxides, or alcohol as the oxidant [3,4]. Oxidants tend to bond to group III atoms on III–V semiconductors since the group III metal atoms are good electron donors and oxidants are good electron acceptors. Nearly all III–V surfaces have tricoordinated group III atoms, which can make single bonds to oxidants. Dissociative chemisorption of  $\text{H}_2\text{O}$  on III–V surfaces would produce hydroxyl, which can be ex-

pected to form single bonds to the group III atoms on the surface with little substrate lattice disruption at low temperature and low coverage. Conversely, oxygen atoms nearly always make two bonds. Therefore, dissociative chemisorption of  $\text{O}_2$  creates surface oxygen atoms that may displace substrate atoms in order to form multiple bonds to the surface metal atoms even at 300 K. During MBE or ALD growth of gate oxides, oxygen may be present in the process environment and so it is essential to understand the reaction of oxygen with the materials involved in transistor fabrication.

The focus of this study is the reaction of molecular oxygen with the group III-rich  $\text{InAs}(001)-(4 \times 2)/c(8 \times 2)$  surface. The  $(2 \times 4)$  series of reconstructions for  $\text{InAs}(001)$  closely resembles the  $(2 \times 4)$  series of surface reconstructions for  $\text{InGaAs}(001)$  [5] and the same nomenclature is employed. These include the As-rich  $\beta 2(2 \times 4)$  and  $\alpha 2(2 \times 4)$  reconstructions, which are stable at lower temperatures and contain arsenic dimers on the 1st row of the surface. The  $\beta 2(2 \times 4)$  structure is more stable at higher As overpressure [6,7]. At higher temperatures and lower arsenic flux, a transition to the In-rich  $(4 \times 2)/c(8 \times 2)$  reconstruction is observed [8,9] which consists of In rows along the  $[110]$  direction separated by ~17 Å. The In-rich  $(4 \times 2)/c(8 \times 2)$  reconstruction has a trough structure that contains two In dimers per unit cell, as shown in Fig. 1. Studies have shown that InGaAs exhibits In surface segregation, which may mean that the  $\text{InGaAs}(001)$  surface layer is almost pure  $\text{InAs}(001)$  [10–12].  $\text{InGaAs}(001)-(4 \times 2)/c(8 \times 2)$  is being extensively investigated for use in III–V MOSFETs [13–15],

\* Corresponding author. Tel.: +1 858 534 3368; fax: +1 858 534 2063.

E-mail addresses: [jclemens@ucsd.edu](mailto:jclemens@ucsd.edu) (J.B. Clemens), [sbishop@ucsd.edu](mailto:sbishop@ucsd.edu) (S.R. Bishop), [dfeldwinn@engineering.ucsb.edu](mailto:dfeldwinn@engineering.ucsb.edu) (D.L. Feldwinn), [rdroopad@txstate.edu](mailto:rdroopad@txstate.edu) (R. Droopad), [akummel@ucsd.edu](mailto:akummel@ucsd.edu) (A.C. Kummel).

<sup>1</sup> Present address: ECE Department, University of California, Santa Barbara, CA 93106-9560, USA.

<sup>2</sup> Present address: Department of Physics, Texas State University-San Marcos, San Marcos, TX 78666, USA.

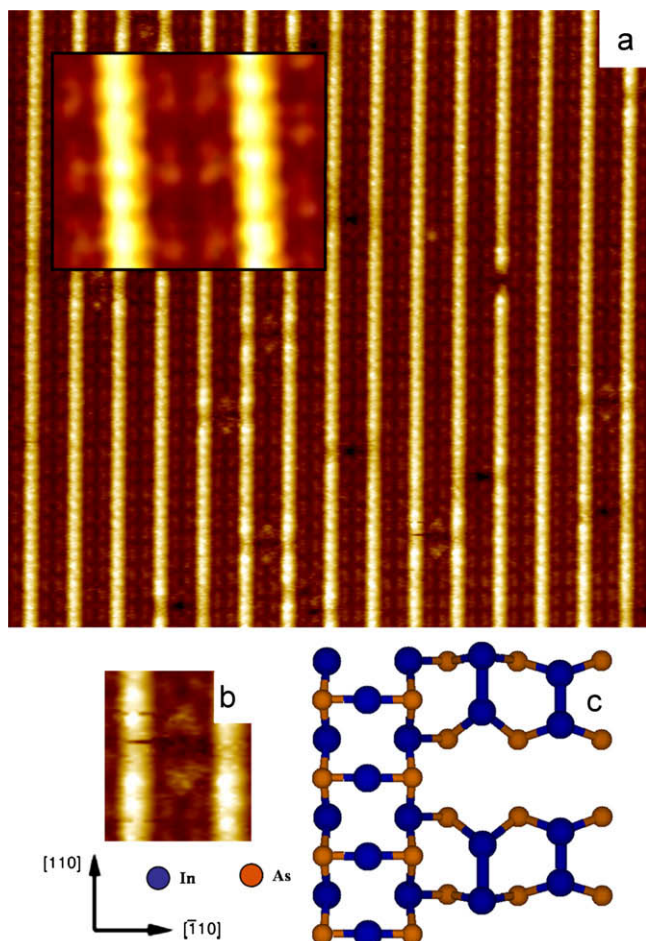


**Fig. 1.** The  $\beta'3'(4 \times 2)$  surface reconstruction of InAs(001). The rows in the  $[110]$  direction consist of In chains and the trough features contain two In dimers per surface unit cell. (a) Filled state STM image ( $-1.50$  V,  $50$  pA,  $260 \times 260$  Å) and detailed inset. (b) Detail of the transitional defect, “T”. (c) DFT ball-and-stick diagram of the InAs(001)- $(4 \times 2)$  surface. The experimental results reproduce the main features shown in the DFT ball-and-stick diagram.

but since InAs(001)- $(4 \times 2)/c(8 \times 2)$  is nearly identical to InGaAs(001)- $(4 \times 2)/c(8 \times 2)$ , it is ideal for atomistic studies of surface reactions since it exhibits much better long-range surface order. Furthermore, InAs has a simpler unit cell compared to InGaAs for DFT simulations.

For dissociative chemisorption of  $O_2$ , electron density from the substrate is likely donated to the incoming oxygen molecule. This process has been shown to occur for the reaction of  $O_2$  on transition metal surfaces [16–18]. In these cases, an  $O_2^-$  or  $O_2^{2-}$  molecularly chemisorbed species is formed via electron donation from the metal surface, which precedes dissociative chemisorption. The donation of electron density to  $O_2$  upon the chemisorption on Si(001) surfaces has also been shown to occur [19,20] and it is postulated that the density would occupy the  $\pi^*$  antibonding orbital of the  $O_2$  molecule prior to dissociative chemisorption [21], initiating the breaking of the oxygen molecular bond. The overall process on InAs(001)- $(4 \times 2)/c(8 \times 2)$  is likely very similar. It has been shown on the GaAs(001)- $(2 \times 4)/c(2 \times 8)$  surface that As dimers provide electron density for  $O_2$  dissociative chemisorption even though the final oxidation product on the surface is insertion of O atoms into the As–Ga backbonds and subsequent As displacement [22]. Oxidation of the As-rich GaAs(001)- $(2 \times 4)/c(2 \times 8)$  and GaAs(001)- $(6 \times 6)$  surfaces by molecular oxygen proceeds via the displacement of surface arsenic atoms, lead-

ing to surface Fermi level pinning [23,24]. This is consistent with  $Ga_2O_3$  being more thermodynamically stable than arsenic oxides. For reaction of InAs(001) with  $O_2$ ,  $In_2O_3$  is also expected to be the most thermodynamically stable oxide [25,26]. Therefore, it can be expected that oxidation of the InAs(001)- $(4 \times 2)/c(8 \times 2)$  surface proceeds via a similar mechanism whereby the  $O_2$  is initially attracted to the electron density at the nearly filled (empty) surface As (In) dangling bonds, then proceeds to form more thermodynamically stable In–O bonds, potentially displacing surface arsenic.

InAs(001)- $(4 \times 2)/c(8 \times 2)$  has no surface As dimers so dissociative chemisorption on this reconstruction is expected to be highly activated. The  $\beta'3'(4 \times 2)$  reconstruction is shown in Fig. 1. This surface reconstruction has only the row-edge As atoms as electron-donor sites [27]. Tricoordinated surface In atoms or *sp*-hybridized dicoordinated In atoms of the  $\beta'3'(4 \times 2)$  reconstruction of InAs(001) would be expected to have nearly empty dangling bonds based on simple electron counting models [28]. Existing experiments on other InAs surfaces support this hypothesis. The InAs(011) surface has no As dimers [29,30] and exhibits an initial sticking probability of less than  $10^{-5}$  for molecular oxygen [31]. Studies of the low temperature oxidation of InAs(001) have shown that the anion-rich surface, or the  $(4 \times 2)$  reconstruction, is much less reactive to molecular oxygen than the cation-rich surface, or the  $(2 \times 4)$  reconstruction [32]. Since there are no surface As dimers on InGaAs(001)- $(4 \times 2)/c(8 \times 2)$  or InAs(001)- $(4 \times 2)/c(8 \times 2)$ , these surfaces are more likely to be optimal for the starting template for ALD of gate oxides.

## 2. Methods

### 2.1. Experimental setup

Experiments were performed in a UHV chamber with a base pressure of  $2 \times 10^{-11}$  Torr. The chamber was equipped with an Omicron low temperature scanning tunneling microscope (STM) and an Omicron SpectraLEED low energy electron diffractometer. Highly doped 300 nm thick InAs layers were grown by collaborators offsite by MBE on commercially available InAs substrates. The doping concentration was  $1 \times 10^{18}$   $cm^{-3}$  for both n-type and p-type wafers, using either Si or Be as dopants. The InAs samples were protected with a 60–80 nm thick amorphous  $As_2$  capping layer for transport. After transfer into the UHV analysis chamber, the InAs samples were degassed at  $200$  °C for 3 h and then heated to  $380$  °C for 2 h to desorb the  $As_2$  capping layer. The desired InAs(001)- $(4 \times 2)/c(8 \times 2)$  reconstruction was obtained by increasing the substrate temperature by  $0.2$  °C  $s^{-1}$  to  $450$  °C and holding for 10 min. Surface periodicity was confirmed using LEED and STM. Oxygen dosing was performed *in situ* at  $20$ – $25$  °C through a UHV leak valve at pressures from  $2 \times 10^{-8}$  to  $2 \times 10^{-6}$  Torr. Some STM images were acquired during  $O_2$  dosing to differentiate oxygen-induced sites from defect sites on the InAs(001)- $(4 \times 2)/c(8 \times 2)$  surface and to observe the evolution of the oxygen chemisorption sites with increasing  $O_2$  exposure. Additional STM images were obtained in the absence of  $O_2$  after background dosing by  $O_2$ . Filled state STM images were acquired at  $-1.50$  V to  $-2.00$  V sample bias relative to the electrochemically etched W tip. The constant-current images were taken at a tunneling current setpoint of 100 pA.

### 2.2. Computational details

The experimental results were confirmed with density functional theory (DFT) calculations. The Vienna *ab-initio* simulation package (VASP) code was used with plane wave calculations and

periodic boundary conditions [33,34]. A slab consisting of nine atomic layers was employed with termination on the bottom surface by H atoms with a charge of  $1.25 e^-$ . The bottom three layers of the slab, along with the H atoms were frozen in the bulk position in order to preserve the bulk properties of the system. The vacuum consisted of thirteen layers, which minimized the interaction of the top and bottom layers of the slab. The calculations were performed with the Perdew–Burke–Ernzerhof (PBE) [35] variant of the generalized gradient approximation (GGA) and the atoms were modeled using the projector augmented wave (PAW) [36] potentials that were supplied with VASP. The generation of four irreducible k-points in the first Brillouin zone was achieved by using  $2 \times 4 \times 1$  Monkhorst–Pack k-point sampling scheme. The plane wave cutoff energy was 500 eV and the criteria for full relaxation and termination of the calculations was when the forces were less than  $0.05 \text{ eV/\AA}$ . VASP was used for geometry relaxations and adsorption energies.

To verify the autocatalytic dissociative chemisorption, a Monte Carlo simulation of the site size distribution for  $\text{O}_2$  on  $\text{InAs}(001)-(4 \times 2)/c(8 \times 2)$  was developed using MATLAB, version 7.4.0 R2007a. A numerical simulation of the number of available chemisorption sites for  $\text{O}_2$  was created that represented the number of available sites on the  $\text{InAs}(001)-(4 \times 2)/c(8 \times 2)$  surface observed in STM. Only In-row chemisorption sites were allowed because  $\text{O}_2$  sticking in the trough was not observed. Initial chemisorption sites were chosen randomly and given a weighted probability for the relative sticking coefficient,  $0 \leq s \leq 1$ . For  $s = 1$ , the simulated sites resulted from a single oxygen molecule impinging on the InAs surface and reacting at that location with the chemisorption of a single O atom. Other factors, such as the sticking probability of impinging  $\text{O}_2$  molecules adjacent to already-oxidized sites, were considered and are described in Section 3.2. The sites were analyzed by measuring their lengths and developing an average distribution of O chemisorption site lengths over 100 or more simulations. The weighted sticking probability allowed for tailoring different site-length distributions. These results were compared to an equivalent area of the real oxidized surface.

### 3. Results and discussion

#### 3.1. Experimental results

The clean surface of  $\text{InAs}(001)-(4 \times 2)/c(8 \times 2)$  has been imaged using STM by other researchers [8,9,37], but new features have been observed recently [27]. The main features of the  $\text{InAs}(001)-(4 \times 2)/c(8 \times 2)$  are rows of In atoms along the  $[110]$  direction and trough regions in between the row features that con-

tain two In–In dimers per unit cell in the 3rd atomic layer. The rows are spaced  $17.2 \text{ \AA}$  apart, and the trough dimer-to-dimer distance in the  $[110]$  direction is  $8.6 \text{ \AA}$ . This structure is shown in Fig. 1 and is called the  $\beta_3'(4 \times 2)$  reconstruction of the  $\text{InAs}(001)$  surface. The  $c(8 \times 2)$  periodicity arises from the superposition of  $(4 \times 2)$  unit cells, with the shift of  $\frac{1}{2}$  unit cell (or  $4.3 \text{ \AA}$ ) in the  $[110]$  direction between neighboring  $(4 \times 2)$  regions. The shift initiates at the trough-region defects called transitional defects, or “T”, as shown in Fig. 1b [9].

Upon imaging the  $\text{O}_2$  dosed  $\text{InAs}(001)-(4 \times 2)/c(8 \times 2)$ , two major types of In row oxygen adsorption sites are observed: dark cuts in the In row or grouped bright protrusions atop the In row, as shown in Fig. 2. The STM images in Fig. 2 shows  $\text{InAs}(001)-(4 \times 2)/c(8 \times 2)$  after 500 L of  $\text{O}_2$ . Depending on STM tip conditions, either one type of site or the other is observed, but not both concurrently. Modification of STM image contrast due to tip functionalization is a common phenomenon [38–41]. Excess arsenic leftover from the capping/decapping procedure and adsorbed oxygen are both present on the InAs surface. Either excess As or O atoms could cause a functionalization of the tungsten tip consistent with the observed adsorption site image contrast reversal.

Sticking was absent in the trough regions for these O coverages, verified when high resolution tunneling conditions were acquired. The sticking probably was estimated by counting the number and sizes of adsorption sites on the surface from the STM images. From each of the images in Fig. 2, the sticking probability was estimated to be  $1.3 \times 10^{-4}$ . A sticking probability of  $\sim 1.6 \times 10^{-4}$  was measured from STM data from a repeated experiment. The measured sticking probability is slightly higher than the sticking probability for the cleaved  $\text{InAs}(011)$  surface measured by MacRae and coworkers [31]. However, the  $(011)$  surface of InAs is more polar than the  $(001)$  surface of InAs, and it contains no In–In bonds nor dicoordinated In atoms.

##### 3.1.1. The dark-site imaging condition

The most common  $\text{O}_2$  chemisorption sites seen in STM under the dark-site imaging condition after  $\sim 500 \text{ L}$  exposure on  $\text{InAs}(001)-(4 \times 2)/c(8 \times 2)$  are shown in Fig. 3a–c. These sites appear as cuts in the In rows in the  $[110]$  direction and are labeled as single, double, and triple cuts. At these exposures, the most common O dark site has a length along the row of about  $21\text{--}24 \text{ \AA}$  (a double cut). This corresponds to a distance equivalent to  $2.5\text{--}3$  unit cell lengths in the  $[110]$  direction, or the length of  $5\text{--}6$  In atoms along the row.

STM images in dark-site conditions were acquired during the oxidation of the InAs surface as shown in Fig. 4. The initial oxidation site forms after about  $20 \text{ L}$  of exposure to  $\text{O}_2$  at a pressure of

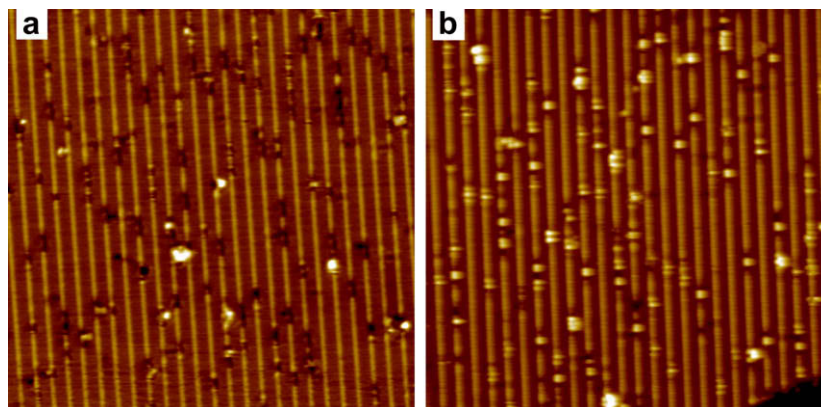


**Fig. 2.** The  $\text{InAs}(001)-(4 \times 2)/c(8 \times 2)$  surface after oxidation by  $\text{O}_2$  at a dose of  $\sim 500 \text{ L}$ . (a) Filled state STM image under the dark-site imaging condition. (b) Filled state STM image under the bright-site imaging condition. STM images ( $440 \times 440 \text{ \AA}$ ) acquired at  $-2.0 \text{ V}$ ,  $100 \text{ pA}$ .

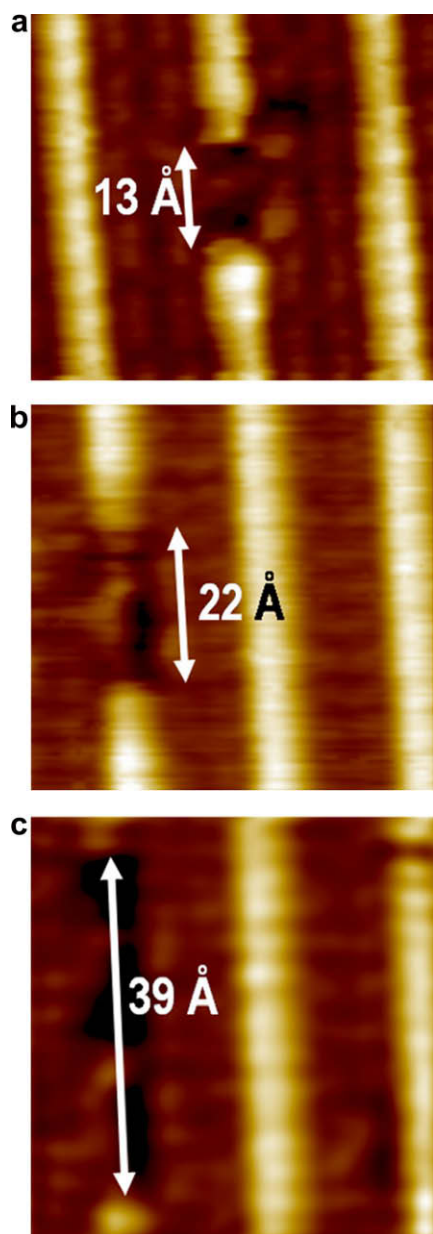


**Fig. 3.** Detail of the  $O_2$  chemisorption sites observed in STM with the dark-site imaging condition. (a) The single cut site. (b) The double cut site. (c) One of several larger cut sites.

$2 \times 10^{-8}$  Torr and has a measured length of about 12 Å (Fig. 4b). After 50 L of total  $O_2$  exposure, the reaction site increases in length to about 24 Å (Fig. 4c). The line scans along these sites in Fig. 4d show the evolution of oxygen chemisorption. Using filled state STM images of the clean surface, the apparent height difference between the top of the In row and the top of the In–In dimer in the trough is about 1.5 Å. At submonolayer coverages of  $O_2$ , the dark cuts in the filled state STM image appear to have a depth of 1.5–2 Å below the row height (slightly deeper than the trough).

The experiments are consistent with the initial oxygen sites on the In row of the InAs(001)-(4 × 2)/(8 × 2) surface acting as nucleation centers for further chemisorption of molecular oxygen. The site length of ~24 Å remained unchanged in length until a final dose of 150 L. The 24 Å site length correlates to the most common length of observed sites in large scale images after even higher exposures of up to 500 L; therefore, it is hypothesized that the 24 Å site is the most stable oxidation sites for these conditions.

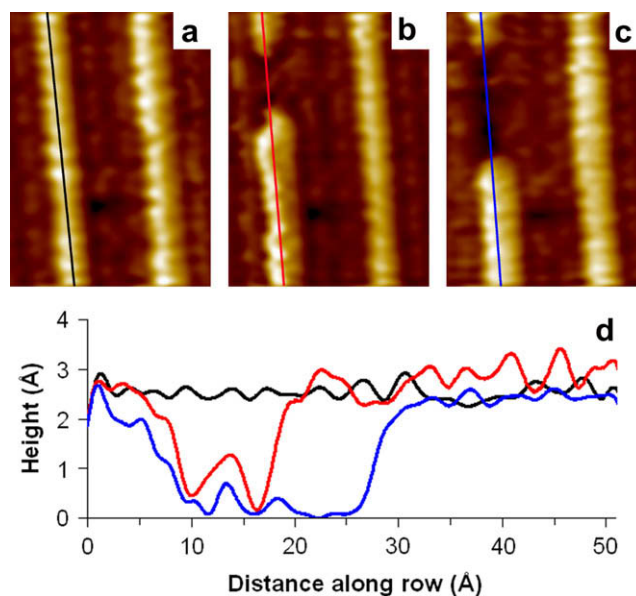


**Fig. 4.** The evolution of a single oxidation site on the InAs row under dark-site imaging condition. The  $52 \times 35$  Å filled state STM images ( $-2.0$  V, 100 pA) were taken during continuous oxidation ( $O_2$  background pressure =  $2 \times 10^{-8}$  Torr). (a) Before the  $O_2$  dose. (b) Same area of surface after  $O_2$  dose of 20 L. (c) Same area of surface after 50 L  $O_2$  dose. (d) The line scan data for Fig. 4a (black), Fig. 4b (red), and Fig. 4c (blue). (For interpretation of the references to colour in this figure legend, the reader is referred to the web version of this article.)

The smallest site observed after  $O_2$  exposure is ~4 Å long and this could be due to a single O atom. If oxygen chemisorption takes place on the surface in a random non-autocatalytic fashion, it would have Poisson spatial distribution; therefore at low coverage, the number of single sites would be the greatest, followed by double sites, and then triple sites, etc. Since  $O_2$  dissociates into pair of O atoms, one might expect the double site to be most common. This is indeed observed experimentally that few small ~4 Å sites are seen. However, STM images reveal that the greatest number of sites have an apparent length of ~24 Å. This strongly suggests that there is an energetic stability in forming adjacent oxygen sites for more than two O atoms.

### 3.1.2. The bright-site imaging condition

When the other imaging condition is observed, the  $O_2$  chemisorption sites are imaged as bright protrusions. The protrusions show three main types of sites occurring: the “pyramid,” the “doublet,” the “quad” sites shown in Fig. 5a, b, and c, respectively. Larger sites also occur more infrequently, but the shapes of these sites vary greatly. The pyramid site has an apparent length of 27 Å and an apparent height of 1.0–1.2 Å from the center of the site to the top of the In row. The doublet sites are slightly taller with an apparent height of 1.1–1.3 Å and a length of 21 Å, including the surrounding dark regions. The quad site consists of a cluster of protrusions, with a height of 1.5–2.0 Å and a length of about 27 Å.

Oxidation during STM was also carried out under the bright-site imaging condition. This allowed for the identification of initial  $O_2$  sites and their evolution under continued  $O_2$  exposure. The evolution of the oxidation of the InAs surface is shown in the filled state STM images in Fig. 6. In Fig. 6a, the  $O_2$  exposure is 50 L and there are two pyramid sites already present, labeled 1 and 2. After 150 L exposure, site 1 has developed into a doublet site while site 2 remains a pyramid site. In Fig. 6c, the  $O_2$  exposure is 550 L. Site 1 remains a doublet, site 2 appears to have developed into a doublet-like state, and there are two new pyramid sites, labeled 3 and 4. Fig. 6d was acquired after the  $O_2$  exposure reached its final value

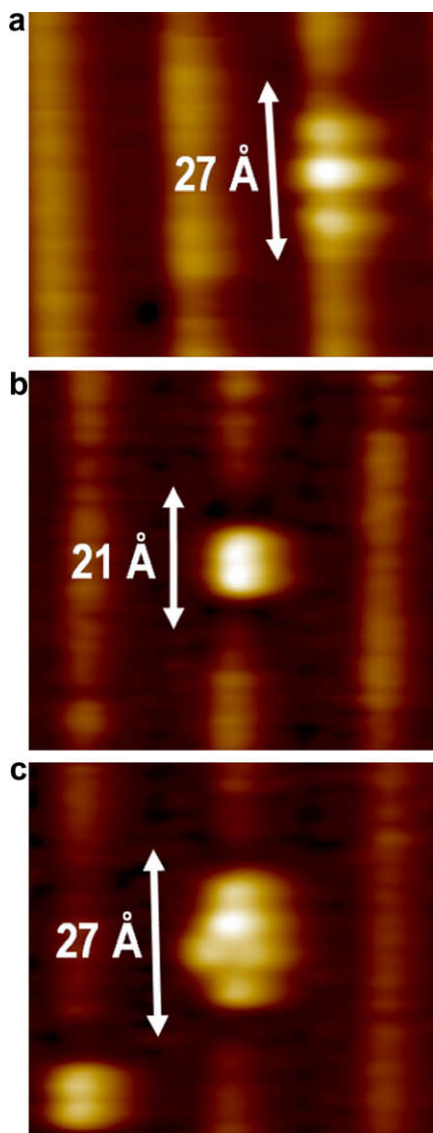


**Fig. 5.** Detail of the  $O_2$  chemisorption sites observed in STM with the bright-site imaging condition. (a) The pyramid site. (b) The doublet site. (c) The quad site.

of 1020 L. In this image, site 3 has now evolved from a pyramid to a doublet, site 1 remains a doublet, site 2 remains doublet-like, and site 4 remains a pyramid. The pyramid sites are the first STM evidence of  $O_2$  chemisorption, and they almost always evolve into doublet sites. It was not observed that a doublet site evolved into a pyramid site under  $O_2$  exposure.

The initial oxygen chemisorption site observed on  $InAs(001)-(4 \times 2)c/(8 \times 2)$  under the dark-site imaging condition was shown to be the In row single cut in Figs. 3a and 4b. It is reasonable to assume that the equivalent in the bright-site imaging condition is the pyramid site. Additionally, the equivalent of the doublet in dark-site imaging conditions would most likely be the double cut site shown in Figs. 3b and 4c. The pyramid and the doublet have very similar lengths in STM of 24 Å and 21 Å, respectively. However, the single cut and double cut sites have lengths of 13 Å and 22 Å, respectively. The “pyramids” consist of a more prominent center circular area and two flanking, less prominent areas that appear less well defined. The development of the pyramid site into the doublet site involves little change in the overall length of the site. It involves creating another circular area of equal prominence and adjacent to the original central feature in the pyramid. This is in

contrast to the dark-site imaging condition in which the site actually grows unidirectionally with further oxidation. This suggests that the flanking features to the central prominence of the pyramid site are electronic effects.

### 3.2. Site size distribution simulation

Since at high coverage, single or double sites are no longer the most probable sites even for a Poisson spatial distribution, a Monte Carlo simulation was performed to predict the distribution of oxygen sites at the experimentally observed coverage. Fig. 7a is the oxygen chemisorption site length distribution that results from the experimental STM data from Fig. 2a. The same STM image is shown in Fig. 7b. If an equivalent oxygen coverage is instead distributed randomly as single O sites, a Poisson spatial distribution predicts an exponential-like decay of site sizes, with the maximum number of sites being at the length of about 4 Å. The results of this simulation are shown in the site length distribution in Fig. 7c, with a pictorial representation in Fig. 7d. Fig. 7e comes from a weighted simulation in which there was a greater probability for a new O site to bond near a pre-existing site. The probability of sticking to a site without any neighboring sites being occupied (an isolated O chemisorption site) can be adjusted by applying a relative sticking factor of 0–1. The relative sticking probability for an isolated site was set to 0.10, while the relative sticking probability for an adjacent (immediately next to an already-occupied site) was set to unity or 1.00. This resulting O site distribution for weighted sticking is represented pictorially in Fig. 7f. It still does not match the experimental distribution. The distribution in Fig. 7g results from the attempted reproduction of the experimental data. The clean surface relative sticking probability is set to 0.01 in this simulation and the adjacent-site sticking probability is set to unity. There was also a soft limit on the length of sites that were generated. This was done by setting the relative sticking probability to 0.07 for all sites that would result in an overall site length of greater than 24 Å. The purpose of these parameters was to reproduce the maximum from the experimental sets of data that all showed the most common site size to be about 21–24 Å for the observed coverage. The pictorial representation of this simulation is shown in Fig. 7h. This case reproduces most closely the experimental data. It gives a maximum at frequency  $\cong 30$  at a site length of about 24 Å.

This simple model allows one to estimate the relative difference in sticking probabilities for the isolated versus adjacent oxygen chemisorption sites. Although it does not represent the true sticking probability of  $O_2$  on  $InAs(001)-(4 \times 2)c/(8 \times 2)$ , it does show approximately what the ratio of sticking probabilities should be for isolated to adjacent sites. In the case for Fig. 7g–h, this ratio is 0.01; specifically, the probability of chemisorption of oxygen to isolated sites is approximately 100 times lower than for chemisorption of oxygen adjacent to preexisting oxygen chemisorption sites. The results for the weighted probability distribution can lend insight to the relative activation energy barrier lowering during the autocatalytic effect.

Assuming a simple one dimensional activated chemisorption model for the  $O_2$  bonding to the  $InAs(001)-(4 \times 2)c/(8 \times 2)$  surface, the energy barrier lowering for additional  $O_2$  chemisorption to adjacent sites (autocatalytic effect) can be estimated. For  $O_2$  molecules impinging onto the InAs surface, the translational energy follows the flux-weighted Maxwell–Boltzmann (FWMB) distribution [42,43]. Only  $O_2$  molecules with enough translational energy can overcome the activation barrier to chemisorption on isolated sites. Since the experimental sticking probability is known to be  $10^{-4}$ , this represents only the highest-energy 0.01% of the impinging 300 K  $O_2$  molecules for the simple one-dimensional model. Using integrated areas for a FWMB distribution, these  $O_2$  molecules have a translational energy of at least 0.30 eV. Sticking

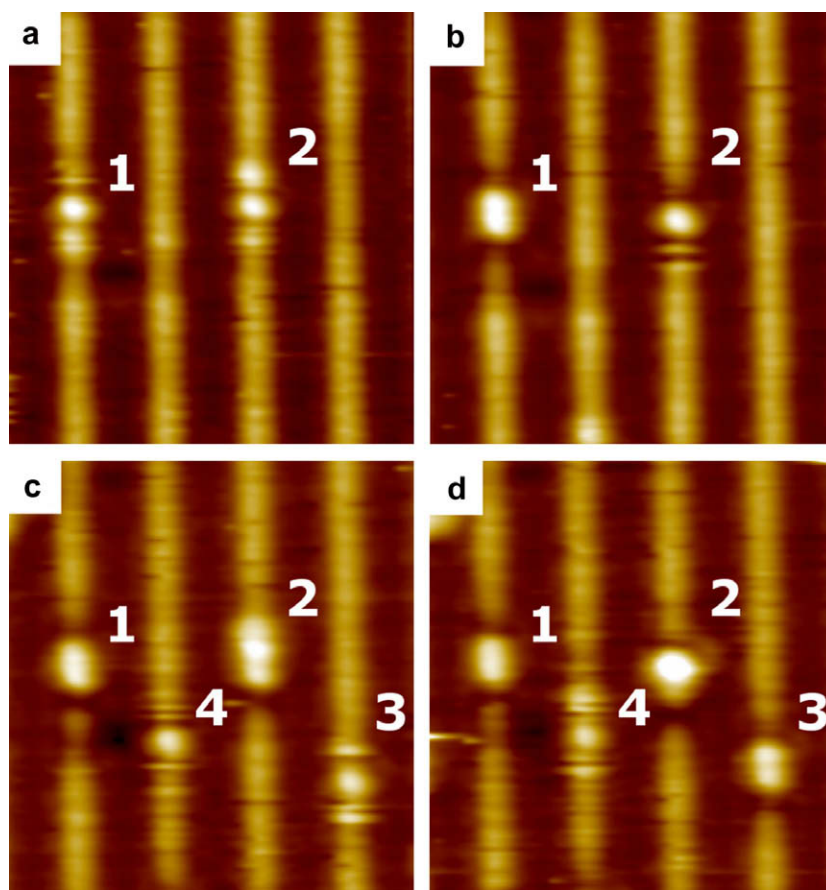


**Fig. 6.** The evolution of several single oxidation sites on the InAs row with the bright-site imaging condition. The  $90 \times 90 \text{ \AA}$  filled state STM images ( $-1.50 \text{ V}$ ,  $100 \text{ pA}$ ) were taken during oxidation ( $\text{O}_2$  background pressure =  $5 \times 10^{-8}$  to  $1 \times 10^{-7}$  Torr). (a) InAs surface after 50 L. (b) Same area of surface after 150 L total dose. (c) After 550 L total  $\text{O}_2$  dose. (d) After 1020 L total  $\text{O}_2$  dose. The evolution from pyramid sites to doublet sites is evident on sites #1–3.

to adjacent O adsorption sites was estimated to be about 100 times greater than to isolated sites. This represents the  $\text{O}_2$  molecules with the highest 1% of translational energy in the FWMB energy distribution. Using integrated areas for a FWMB distribution, the impinging  $\text{O}_2$  molecules would require translational energies of at least 0.17 eV for bonding to adjacent sites. This represents an energy barrier lowering of 0.13 eV from  $\text{O}_2$  binding on isolated versus adjacent sites of the  $\text{InAs}(001)-(4 \times 2)/c(8 \times 2)$  surface.

The barrier lowering could be due to the creation of charge donation centers on the surface. If  $\text{O}_2$  chemisorption results in As displacement, there would be under-coordinated As on the surface. This excess As may become an electron donor to incoming oxygen, thereby lowering the activation barrier to oxidation compared to the clean surface. From the STM images, areas of high charge density are seen, as in the case of the “protrusion” type sites. These sites could offer enough easily accessible electron density for the required 0.13 eV energy barrier lowering. Additionally, as the site sizes become larger, more bright areas are observed in STM. Data from STM is a convolution of both geometric and electronic effects. Therefore it is unknown whether the protrusions are simply electron density from filled non-bonding orbitals, or whether they result from displaced substrate atoms. In either case, it is reasonable to assume that these sites would lower the activation barrier for oxidation. Displaced substrate atoms can result in higher energy partially-filled orbitals. Also, if the protrusions represent electron density in filled state STM images, that electron density could be transferred to the HOMO of an incoming  $\text{O}_2$  molecule. Both of these cases would lower the activation barrier to oxidation.

The combination of a highly exothermic reaction with a low initial sticking probability is consistent with a large activation barrier for  $\text{O}_2$  dissociative chemisorption on  $\text{InAs}(001)-(4 \times 2)/c(8 \times 2)$ . Clustering of the chemisorption sites furthermore indicates that either clustered sites are more thermodynamically stable or there is an autocatalytic process which lowers the activation barrier to  $\text{O}_2$  dissociation near existing O chemisorption sites. Since the chemisorption is highly activated, it is likely that the autocatalytic effect is due to differences in the activation barrier and not chemisorption energy. However, the observation of a maximum in the observed oxygen site length of 21–24 Å suggests a thermodynamic effect.

### 3.3. Density functional theory results

DFT simulations were performed to model the chemisorption sites. The DFT model for  $\text{InAs}(001)-(4 \times 2)$  that was used in this study represents two surface unit cells, as shown in Fig. 1. The distance in the  $[110]$  direction for the unit cell is only 17.2 Å, so it was impossible to accurately reproduce the 21–24 Å sites seen in STM. The DFT results show which sites are possible at the low coverage, initial chemisorption stage due to these computational limitations. STM simulations of the O chemisorption sites were performed but were omitted since simulations of the full 24 Å sites are impossible at the current computational limitations for this model. In addition there is a well documented problem with DFT underestimating the band gaps of semiconductors and insulators [44,45]. In the case of narrow band gap semiconductors such as InAs, the band gap is predicted to be nonexistent. This results in

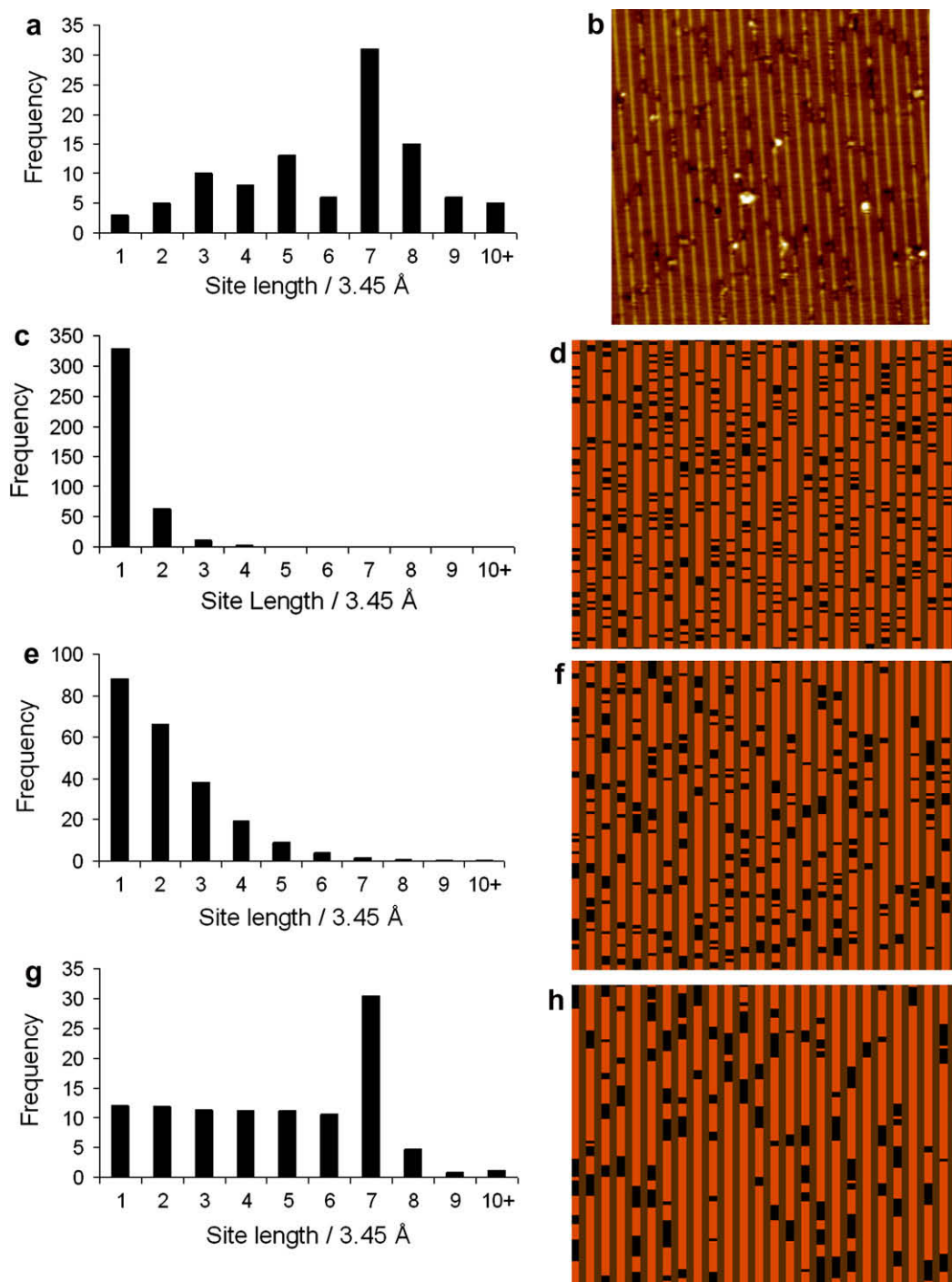


**Fig. 7.** Results for the Monte Carlo simulations and a comparison to the experimental data. (a) The experimentally observed distribution of site lengths from the data in Figs. 2a and 7b with a maximum at 7 (site length of  $\sim 24$  Å). (b) The experimental STM image for the distribution in Fig. 7a. (c) The distribution of site lengths obtained from an average of 100 simulations with a 1.00 sticking probability for all sites. (d) Results from one simulation using conditions described in Fig. 7c. (e) The distribution of site lengths obtained from an average of 100 simulations with a 0.10 sticking probability to isolated sites and a 1.00 probability for sticking to adjacent sites. (f) Results from one simulation using conditions described in Fig. 7e. (g) The averaged data of 100 simulations for a 0.01 sticking probability for isolated sites, a 1.00 sticking probability for adjacent sites, and a sticking probability for sites greater than 24 Å of 0.07. (h) Results from one simulation using conditions described in Fig. 7g.

mixing between the HOMO and LUMO states, which could lead to inaccurate DFT STM simulations. This was reflected in the fact that the empty state DFT STM simulation reproduced the filled state experimental STM results.

There are three main types of oxygen binding sites on InAs(001)-(4 × 2): arsenic displacement sites (Fig. 8a and b), In–In insertion sites (Fig. 8c), and InAs<sub>2</sub> displacement sites (Fig. 8d). For the As displacement site, an oxygen molecule displaces the

row-edge As atoms on the 2nd atomic layer and the displaced As atoms are assumed to form trough As–As dimers. The chemisorbing O<sub>2</sub> molecule can displace As atoms either on the same side or opposite side of the row as shown in Fig. 8a and b, respectively. For the In–In insertion sites, an oxygen atom inserts between the In atoms along the row to form an In–O–In bond. For the InAs<sub>2</sub> displacement, an oxygen molecule displaces a row In atom and the two row-edge As atoms to which it is bonded, leaving the O atoms

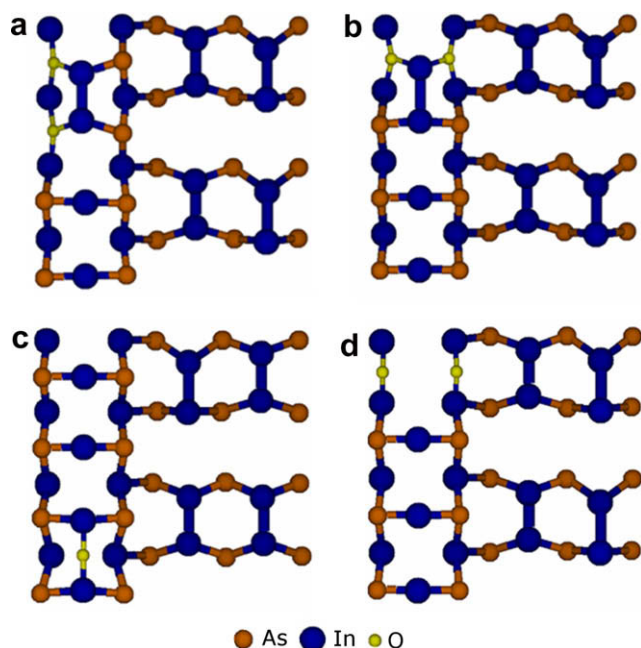


**Fig. 8.** The oxygen adsorption sites examined with DFT. (a) Double As displacement on the same side of the row. (b) Double As displacement on opposite sites of the row. (c) The In–In insertion site. (d) The  $\text{InAs}_2$  displacement site. These DFT ball-and-stick diagrams show only the top 3 atomic layers of the simulated slabs and the displaced atoms are not shown for clarity.

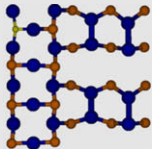
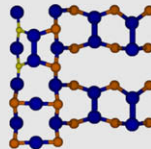
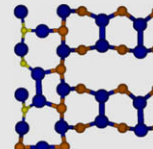
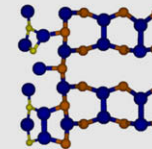
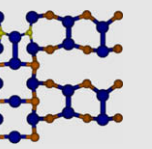
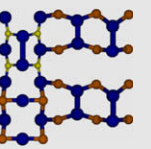
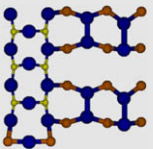
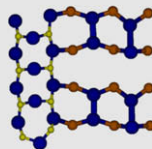
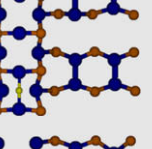
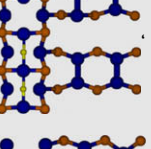
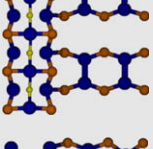
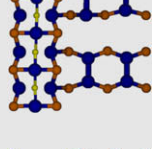
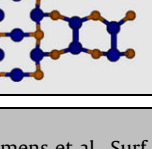
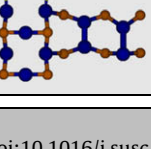
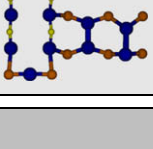
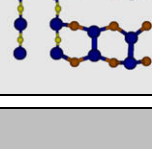
in the sites previously occupied by As and a cut in the row; the displaced  $\text{InAs}_2$  are assumed to form a pyramid site in the trough. The displaced atoms are not shown in Fig. 8 in order to more clearly see

the resulting O chemisorption sites. It is important to note that the O adsorption sites could have different apparent lengths in the experimental STM images. For instance, a single O into the In–In insertion site would appear about as long in the  $[1\ 1\ 0]$  direction as two adjacent opposite side-of-row As displacements by 2 O atoms. Either of these could correspond to the smallest 4 Å site observed experimentally.

The number of consecutive insertion and displacement sites was also examined. Using the slab model for InAs, it was possible to model one, two, three and infinite insertion and displacement sites. This is due to the size of the InAs slab, which contains two surface unit cells, and the periodic boundary conditions. The DFT calculations of the binding sites for O onto  $\text{InAs}(0\ 0\ 1)-(4 \times 2)$  show that there are a multitude of stable binding sites with exothermic enthalpies of adsorption, ranging from  $-0.5$  to  $-2.0$  eV (see Table 1).

The most reactive As atoms on the surface are those at the row edge because they form only three bonds to the substrate, leaving a dangling bond with electron density. Displacement can occur either on the same side or the opposite side of the row. The As displacement sites are shown to be thermodynamically stable, with nearly degenerate energies, regardless of the number of As displacements. The stability for all of the displacement sites is about  $-2$  eV per O. However, there is a slight trend towards greater stability with greater number of As displacements by O for displacement on the same side of the row, as indicated in Table 1, row 1. The single As displacement is stable by  $-1.40$  eV and the stability increases for the infinite displacement which is stable by  $-2.15$  eV. This trend supports the thermodynamic driving force for the formation of large sites. However, As displacement on opposite sides of the row shows no trend, with all sites energetically equivalent within 0.28 eV as shown in row 2 of Table 1. Additionally, this site would be less likely to occur than the same-side-of-row As

**Table 1**  
Summary of the enthalpies of oxygen chemisorption on  $\text{InAs}(0\ 0\ 1)-(4 \times 2)$ . All energies are per O atom and with respect to the  $\text{O}_2$  molecule and were determined via DFT. Energies are listed towards the right in order of increasing number of adjacent O adsorption sites. In the case of the 2 different As displacement sites, the displaced 2 As form adimers in the trough region. In the last case, the  $\text{InAs}_2$  is displaced and inserts into two In dimer bonds across the trough in the  $[-1\ 1\ 0]$  direction.

Adsorption site	Fig.	$\Delta H_{\text{ads}}$ 1st (eV)	$\Delta H_{\text{ads}}$ 2nd (eV)	$\Delta H_{\text{ads}}$ 3rd (eV)	$\Delta H_{\text{ads}}$ Inf (eV)
Same-side As displacement	8a	 $-1.40$	 $-2.01$	 $-1.73$	 $-2.15$
Opposite-side As displacement	8b	 $-2.10$	 $-1.94$	 $-1.82$	 $-1.91$
In–In insertion	8c	 $-1.77$	 $-1.01$	 $-1.01$	 $-0.45$
$\text{InAs}_2$ displacement	8d	 $-0.86$	 $-0.66$	 $-0.52$	 $-1.06$

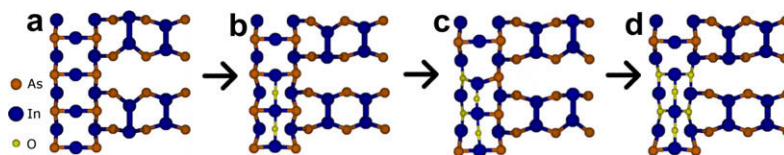


**Fig. 9.** The proposed types of reactions for dissociative chemisorption of  $O_2$  on  $InAs(001)-(4 \times 2)/c(8 \times 2)$ . Fig. 9 is not the result of DFT calculations. (a) The clean surface before oxidation. (b) Oxidation is initiated via In-In insertion by O. (c) As displacement is activated by the In-O-In insertion. (d) The main types of chemisorption sites incorporated into the stable 21–24 Å sites.

displacement sites since an incoming  $O_2$  molecule would need to deposit oxygen atoms on opposite sides of the row.

For the O insertion sites, DFT total energy calculations indicate a trend towards lower stability with increasing site length. The insertion of a single O atom between two row In atoms results in a stabilization energy of  $-1.77$  eV. For the next consecutive O insertion, the stability drops to  $-1.01$  eV per O atom. Finally, with an infinite length O insertion the stability drops off to  $-0.45$  eV per O atom. The energy barrier for subsequent O insertion sites on the In rows may still be lowered (autocatalysis), but there is a limit to the energy gained by further oxidation for insertion sites. For these reasons, the insertion sites would be expected to grow to some limiting site length.

The displacement of an As-In-As group as shown in Fig. 8d is not likely to occur. As shown in Fig. 2, there are two distinct STM imaging conditions during the STM experiment, giving either the “cut” or the “protrusion” features. If an  $InAs_2$  group is displaced from the surface, the existence of cut features in STM images could easily be justified. However, an explanation of how protrusion sites appear in the bright-site imaging condition would be difficult considering the removal of the top two atomic rows in the displacement region. Additionally, the displacement of an  $InAs_2$  group would probably be a very activated process.

It is reasonable to assume that displacement of As from  $InAs(001)-(4 \times 2)/c(8 \times 2)$  is a more activated reaction than for O insertion into the In row atoms. Displacement is usually a multi-step process that proceeds via one or more intermediate steps. Additionally, the electron density at the In atoms on the  $InAs(001)-(4 \times 2)/c(8 \times 2)$  rows is sterically more accessible by incoming  $O_2$  molecules than the dangling bonds of the tricoordinated As atoms in the second atomic layer along the In row. The insertion site is probably the initial reaction site for oxidation of the surface. However, only the first few O insertion sites are exothermic by  $-1.0$  eV or more, so further reaction is suggested via As displacement. Arsenic displacement is stable by about  $-2$  eV, regardless of the number of consecutive adjacent displacement sites.

The overall site size limit is about 24 Å and the autocatalytic mechanism is initiated by insertion. After insertion into the In row, it is suggested that the As displacement mechanism is thermodynamically favored and subsequent reaction can take place via this route, probably resulting in the protrusions seen in bright-site imaging condition. Arsenic atoms on the same side of the row are the likely candidates for displacement. However, as previously stated, the displacement reactions may be more highly activated because displacement proceeds via one or more intermediate steps. Therefore, the sites being limited to 24 Å may be due to an increase in activation barrier as one switches from insertion to displacement sites even though displacement sites are more thermodynamically stable. This overall reaction concept is shown in Fig. 9 in the ball-and-stick diagram. Although not a precise, verifiable mechanism, Fig. 9 illustrates what is believed to take place during oxidation even though it does not include the stable 21–24 Å site.

This proposed mechanism was also modeled by mixing the two main proposed types of oxygen chemisorption sites. Two of the

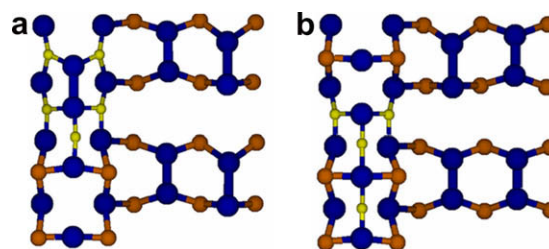


**Fig. 10.** The DFT ball-and-stick diagrams of the mixed O adsorption sites. (a) Four As displacements and one insertion site,  $\Delta H_{ads} = -1.98$  eV. (b) Two As displacements and two insertion sites,  $\Delta H_{ads} = -1.73$  eV. The displaced As atoms are not shown for clarity. Energies are per O atom.

DFT models used are shown in the ball-and-stick diagrams in Fig. 10. In all cases the mixing of insertion and displacement sites was a stable by almost  $-2.0$  eV per O atom, consistent with the proposed mechanism. There was no evidence for thermodynamic limitations of mixing In-In insertion and As displacement sites within the DFT model.

Since dissociative chemisorption of molecular oxygen likely proceeds via transfer of electron density to the  $\pi^*$  antibonding orbital of  $O_2$ , it is possible that there is a low sticking probability on the clean surface because there are no  $1/2$  filled dangling bonds. The autocatalytic effect likely involves the creation of non-bonding orbitals containing electron density that would be reactive towards the  $O_2$  molecule. For example, if the As atoms do not dimerize upon displacement, each As will have two half-filled dangling bonds and should be reactive. The process is similar to what has been observed on  $GaAs(001)-(2 \times 4)/c(2 \times 8)$ , where the electron density of the As atoms is the initial reaction site, but the oxidation results in group-III to oxygen bonds [22,24].

#### 4. Conclusions

Oxidation of  $InAs(001)-(4 \times 2)/c(8 \times 2)$  proceeds via the chemisorption of  $O_2$  onto the rows along the [110] direction. The sticking probability was measured to be very low,  $1-2 \times 10^{-4}$  and the reaction sites tend to be large but finite in size. Oxidation tends to nucleate at a single site and then expand autocatalytically to a size of 21–24 Å. This is consistent with bonding along the In row, occupying about 5–6 In row atom spacings at low oxygen coverage ( $<0.5$  monolayer) and at 23 °C. Monte Carlo simulations show that because the sticking probability is low, the autocatalytic effect could be due to a very small reduction in the activation barrier (0.13 eV) by oxygen-induced displacement of substrate atoms. DFT simulations suggest the initial oxygen binding site is insertion into the In atoms on the rows in the [110] direction, which is stable by  $-1.77$  eV per O atom. However, increasing the number of O insertion sites into neighboring In atoms decreases the stability, consistent with DFT results. The stability of two neighboring row In-In insertion sites is already less stable by 0.76 eV per O atom, limiting the length of the oxidation sites. Further oxidation occurs by displacement of As atoms on

the same side of the rows in the [1 1 0] direction and In–O bond formation, which is stable by about  $-2$  eV per O atom. Bright-site imaging conditions for the largest oxidation sites show what is most likely displaced As. The theoretical results confirm that the growth of the In row insertion sites is ultimately limited by lower stability with increasing length of oxidation sites. Since oxidation of  $\text{InAs}(001)-(4 \times 2)/c(8 \times 2)$  proceeds via an autocatalytic fashion, it is important to limit the amount of oxygen in ALD process systems in order to avoid disruption of the surface lattice during growth.

### Acknowledgements

The authors would like to thank Dr. Ravi Droopad for the fabrication of the InAs wafers used in these experiments. This work was supported by SRC-NCRC-1437.003, and the FCRP-MSD-887.011 and NSF-DMR.

### References

- [1] N. Li, E.S. Harmon, J. Hyland, D.B. Salzman, T.P. Ma, Y. Xuan, P.D. Ye, *Appl. Phys. Lett.* 92 (2008) 143507.
- [2] C.I. Kuo, H.T. Hsu, E.Y. Chang, C.Y. Chang, Y. Miyamoto, S. Datta, M. Radosavljevic, G.W. Huang, C.T. Lee, *IEEE Electron. Dev. Lett.* 29 (2008) 290.
- [3] K. Kukli, K. Forsgren, J. Aarik, T. Uustare, A. Aidla, A. Niskanen, M. Ritala, M. Leskela, A. Harsta, *J. Cryst. Growth* 231 (2001) 262.
- [4] W.S. Jeon, S. Yang, C.S. Lee, S.W. Kang, *J. Electrochem. Soc.* 149 (2002) C306.
- [5] J.M. Millunchick, A. Riposan, B. Dall, C. Pearson, B.G. Orr, *Surf. Sci.* 550 (2004) 1.
- [6] C. Ratsch, W. Barvosa-Carter, F. Grosse, J.H.G. Owen, J.J. Zinck, *Phys. Rev. B* 62 (2000) R7719.
- [7] H. Yamaguchi, Y. Horikoshi, *Jpn. J. Appl. Phys.* 33 (1994) L1423.
- [8] S. Ohkouchi, N. Ikoma, I. Tanaka, *J. Vac. Sci. Technol. B* 12 (1994) 2033.
- [9] C. Kendrick, G. LeLay, A. Kahn, *Phys. Rev. B* 54 (1996) 17877.
- [10] J.M. Moison, C. Guille, F. Houzay, F. Barthe, M. Vanrompay, *Phys. Rev. B* 40 (1989) 6149.
- [11] J.H. Cho, S.B. Zhang, A. Zunger, *Phys. Rev. Lett.* 84 (2000) 3654.
- [12] J.M. Millunchick, A. Riposan, B.J. Dall, C. Pearson, B.G. Orr, *Appl. Phys. Lett.* 83 (2003) 1361.
- [13] M. Passlack, R. Droopad, K. Rajagopalan, J. Abrokwah, R. Gregory, D. Nguyen, *IEEE Electron. Dev. Lett.* 26 (2005) 713.
- [14] I. Ok et al., *Appl. Phys. Lett.* 92 (2008) 202903.
- [15] Y. Xuan, Y.Q. Wu, H.C. Lin, T. Shen, P.D. Ye, *IEEE Electron. Dev. Lett.* 28 (2007) 935.
- [16] D. Kelly, R.W. Verhoef, W.H. Weinberg, *J. Chem. Phys.* 102 (1995) 3440.
- [17] J.E. Davis, P.D. Nolan, S.G. Karseboom, C.B. Mullins, *J. Chem. Phys.* 107 (1997) 943.
- [18] M.C. Wheeler, D.C. Seets, C.B. Mullins, *J. Chem. Phys.* 105 (1996) 1572.
- [19] J.H. Rechten, U. Imke, K.J. Snowdon, P.H.F. Reijnen, P.J. Vandenhoek, A.W. Kleyn, A. Namiki, *Nucl. Instrum. Meth. Phys. Res. Sect. B* 48 (1990) 339.
- [20] T. Miyake, S. Soeki, H. Kato, T. Nakamura, A. Namiki, H. Kamba, T. Suzuki, *Surf. Sci.* 242 (1991) 386.
- [21] Y. Miyamoto, A. Oshiyama, *Phys. Rev. B* 43 (1991) 9287.
- [22] P. Kruse, J.G. McLean, A.C. Kummel, *J. Chem. Phys.* 113 (2000) 9224.
- [23] D.L. Winn, M.J. Hale, T.J. Grassman, J.Z. Sexton, A.C. Kummel, *J. Chem. Phys.* 127 (2007) 134705.
- [24] P. Kruse, J.G. McLean, A.C. Kummel, *J. Chem. Phys.* 113 (2000) 9217.
- [25] J.M. Woodall, J.L. Freeouf, *J. Vac. Sci. Technol.* 19 (1981) 794.
- [26] M. Yamaguchi, A. Yamamoto, H. Sugiura, C. Uemura, *Thin Solid Films* 92 (1982) 361.
- [27] D.L. Feldwinn, J.B. Clemens, J. Shen, S.R. Bishop, T.J. Grassman, A.C. Kummel, R. Droopad, M. Passlack, in preparation.
- [28] M.D. Pashley, *Phys. Rev. B* 40 (1989) 10481.
- [29] A. Schwarz, W. Allers, U.D. Schwarz, R. Wiesendanger, *Phys. Rev. B* 61 (2000) 2837.
- [30] Y. Liang, W.E. Packard, J.D. Dow, H.D. Ho, G.J. Lapeyre, *Phys. Rev. B* 48 (1993) 11942.
- [31] A.U. Macrae, G.W. Gobeli, *J. Appl. Phys.* 35 (1964) 1629.
- [32] V.L. Berkovits, N. Witkowski, Y. Borensztein, D. Paget, *Phys. Rev. B* 63 (2001) 121314.
- [33] G. Kresse, J. Hafner, *Phys. Rev. B* 47 (1993) 558.
- [34] G. Kresse, J. Furthmuller, *Comput. Mater. Sci.* 6 (1996) 15.
- [35] J.P. Perdew, K. Burke, M. Ernzerhof, *Phys. Rev. Lett.* 77 (1996) 3865.
- [36] P.E. Blochl, *Phys. Rev. B* 50 (1994) 17953.
- [37] P. De Padova, P. Perfetti, C. Quaresima, C. Richter, O. Heckmann, M. Zerrouki, R.L. Johnson, K. Hricovini, *Surf. Sci.* 532 (2003) 837.
- [38] L. Bartels, G. Meyer, K.H. Rieder, *Surf. Sci.* 432 (1999) L621.
- [39] B.J. Mcintyre, P. Sautet, J.C. Dunphy, M. Salmeron, G.A. Somorjai, *J. Vac. Sci. Technol. B* 12 (1994) 1751.
- [40] J.R. Hahn, W. Ho, *Phys. Rev. Lett.* 8719 (2001) 196102.
- [41] T. Nishino, P. Buhlmann, T. Ito, Y. Umezawa, *Surf. Sci.* 490 (2001) L579.
- [42] F.M. Zimmermann, W. Ho, *Surf. Sci. Rep.* 22 (1995) 127.
- [43] G. Comsa, R. David, *Surf. Sci. Rep.* 5 (1985) 145.
- [44] J.P. Perdew, M. Levy, *Phys. Rev. Lett.* 51 (1983) 1884.
- [45] L.J. Sham, M. Schluter, *Phys. Rev. Lett.* 51 (1983) 1888.